*Journal of Cluster Science, Vol. 18, No. 3, September 2007 (© 2007)*
DOI: 10.1007/s10876-007-0122-0

# Synthesis and Characterization of the Face-Centered Cubic Clusters $[(Me_3tacn)_8M_8Pt_6(CN)_{24}]^{12+}$ (M = Cr, Mo)

**Lianne M. C. Beltran,[1] Jennifer J. Sokol,[1] and Jeffrey R. Long[1,2]**

*Received February 27, 2007; accepted April 5, 2007; published online July 20, 2007*

Incorporation of a 5*d* transition metal into the face-centered cubic metal-cyanide cluster geometry is accomplished for the first time with the isolation of a series of compounds featuring $[(Me_3tacn)_8M_8Pt_6(CN)_{24}]^{12+}$ (M = Cr, Mo) clusters. Reaction of $[(Me_3tacn)Cr(CN)_3]$ and $K_2[PtCl_4]$ in a boiling aqueous solution generates $[(Me_3tacn)_8Cr_8Pt_6(CN)_{24}]Cl_{12}\cdot 27H_2O$ (**1**), wherein $Pt^{II}$ centers reside at the face-centering sites and the cyanide ligands have reoriented to give $Pt^{II}$–C ≡ N–$Cr^{III}$ linkages. The cyclic voltammogram obtained for a solution of **1** in DMSO exhibits a quasireversible reduction event centered at $E_{1/2} = -1.59$ V versus $Cp_2Fe^{0/1+}$. Reaction of **1** with $K_2[Pt(CN)_4]$ in aqueous solution affords $[(Me_3tacn)_8Cr_8Pt_6(CN)_{24}][Pt(CN)_4]_6\cdot 6H_2O$ (**2**), in which each face of the cubic cluster is capped by a staggered tetracyanoplatinate anion with a Pt–Pt separation of 3.1552(7) Å. Attempts to perform analogous cluster-forming reactions with $[(Me_3tacn)Mo(CN)_3]$ revealed a tendency toward cluster decomposition to give mixtures of insoluble products, including $[(Me_3tacn)_8Mo_8Pt_6(CN)_{24}][Pt(CN)_4]_6\cdot 46H_2O$ (**3**) and $[(Me_3tacn)_8Mo_8Pt_6(CN)_{24}][Pt(CN)_4]_{2.5}[Pt(CN)_3Br]_2Br_3\cdot 6H_2O$ (**4**). Crystallographic analyses revealed these compounds to contain the anticipated $[(Me_3tacn)_8Mo_8Pt_6(CN)_{24}]^{12+}$ cluster in fully- and partially-capped forms, respectively. Unfortunately, the insolubility of these molybdenum-containing products precluded characterization of the cluster by cyclic voltammetry.

**KEY WORDS:** Metal-cyanide clusters; chromium; molybdenum; platinum.

[1]Department of Chemistry, University of California, Berkeley, CA, 94720-1460, USA.
[2]To whom correspondence should be addressed. E-mail: jrlong@berkeley.edu

## INTRODUCTION

Single-molecule magnets are of interest for a variety of potential applications [1] arising from their ability to sustain a remnant magnetization after their removal from a polarizing field. This unusual property stems from the presence of a high-spin ground state with a negative axial zero-field splitting that creates an energy barrier to spin reversal. Despite the discovery of many new species exhibiting such behavior, the highest spin-reversal barrier encountered to date is just 60 $cm^{-1}$ [2], only slightly larger than that observed for the original single-molecule magnet, $[Mn_{12}O_{12}(CH_3CO_2)_{16}(H_2O)_4]$ [3]. In hopes of developing synthetic strategies towards single-molecule magnets with significantly increased blocking temperatures, we are exploring new methods for generating high-spin molecules.

Although most of the efforts toward new single-molecule magnets have involved oxo-bridged systems [4], increasing attention has been devoted to cyano-bridged species [5–7]. Cyanide tends to form linear bridges connecting just two metal centers. Combined with multidentate ligands to limit growth in selected directions, cyanometalate chemistry can target discrete, polynuclear species. For example, facially tridentate blocking ligands (L-*fac*) direct the following assembly reaction towards octanuclear cubic clusters [6, 7]:

$$4\left[(\text{L-}fac)\text{M}(\text{CN})_3\right]^{y-} + 4\left[(\text{L-}fac)\text{M}'(\text{H}_2\text{O})_3\right]^{x+} \rightarrow \left[(\text{L-}fac)_8\text{M}_4\text{M}'_4(\text{CN})_{12}\right]^{4(x-y)+} \quad (1)$$

The eight metal ions of the cluster reside on the corners of a cube and are linked together by linear cyanide bridges. A large variety of these simple cubic $M_4M'_4$ species exist with different metal ions and various blocking ligands, illustrating the well-established feature of metal-cyanide chemistry in which the metal sites of the framework are accommodating to an assortment of metal ions. Once a scaffold is known to be stable, different metals can be incorporated so as to vary the properties of the cluster. While high-spin $M_4M'_4$ species have been isolated [7], larger spins could be attained in systems with more metal sites.

By modifying reaction 1 such that only one reagent contains a blocking ligand, a larger face-centered cubic cluster framework can be attained [7a, 8–10]:

$$8\left[(\text{L-}fac)\text{M}(\text{CN})_3\right]^{y-} + 6\left[\text{M}'(\text{H}_2\text{O})_6\right]^{x+} \rightarrow \left[(\text{L-}fac)_8\text{M}_8\text{M}'_6(\text{CN})_{24}\right]^{(6x-8y)+} \quad (2)$$

In this system, the eight M ions are at the corners of a cube and the six M′ ions lie just above the faces of the cube. This structure was first observed in the clusters $[(Me_3tacn)_8M_8Ni_6(CN)_{24}]^{12+}$ (M = Cr [8a], Mo [9]), wherein the blocking ligand is $Me_3tacn$ = *N*,*N*′,*N*″-trimethyl-1,4,7-triazacyclononane. Here, the face-centered $Ni^{2+}$ ions exhibit square planar coordination, giving rise to a diamagnetic electron configuration. From more recent investigations using other L-*fac* blocking ligands, these sites are now known to also accommodate five-coordinate [7a, 10a,c] or six-coordinate [10b] metal ions. This has led to some high-spin $M_8M'_6$ species [10], including $[(Tp)_8(H_2O)_6Cu_6Fe_8(CN)_{24}]^{4+}$, in which the blocking ligand is $Tp^-$ = hydrotris(pyrazol-1-yl)borate and the $Cu^{2+}$ ions exhibit square pyramidal coordination [10a]. Although the $S = 7$ ground state cluster possesses a negative axial anisotropy, its barrier to spin-reversal could not be measured at temperatures down to 1.8 K employing AC field switching frequencies of up to 1500 Hz [10a].

Despite containing diamagnetic $Ni^{II}$ centers, the face-centered cubic cluster $[(Me_3tacn)_8Mo_8Ni_6(CN)_{24}]^{12+}$ was noted to be of particular interest for its electrochemical behavior [9]. A cyclic voltammogram of the cluster in DMF showed a sequence of six reduction waves spaced approximately 110 mV apart. Comparison with the voltammogram of $[(Me_3tacn)Mo(CN)_3]$ suggests that these events are associated with reductions occuring at the $Mo^{III}$ centers. The behavior raises the possibility that electron transfer between molybdenum sites in a mixed-valence species such as $[(Me_3tacn)_8Mo_8Ni_6(CN)_{24}]^{11+}$ might lead to a high-spin ground state via a double-exchange mechanism analogous to that occurring in Prussian blue [11]. Unfortunately, the close spacing of the redox couples prevents ready isolation of the one-electron reduced cluster, owing to disproportionation. It was hypothesized, however, that replacement of $Ni^{II}$ with $Pt^{II}$ might enhance overlap within the intervening orbital pathway, facilitating electron exchange, and thereby spreading out the reduction waves in energy. Herein, we present our efforts to test this hypothesis, with the synthesis and characterization of the face-centered cubic clusters $[(Me_3tacn)_8M_8Pt_6(CN)_{24}]^{12+}$ (M = Cr, Mo).

## EXPERIMENTAL

### Preparation of Compounds

$[(Me_3tacn)Cr(CN)_3]$ [8] and $[(Me_3tacn)Mo(CN)_3]$ [9] were prepared as previously reported, and $K_2[PtCl_4]$, $K_2[PtBr_4]$, and $K_2[Pt(CN)_4]$ were purchased from commercial sources. Only distilled, de-ionized water was used in the following syntheses. Other solvents were obtained commercially and used as received, unless otherwise noted.

*[(Me$_3$tacn)$_8$Cr$_8$Pt$_6$(CN)$_{24}$]Cl$_{12}$·27H$_2$O (1)*

A 15-mL aqueous solution of $K_2[PtCl_4]$ (398 mg, 0.959 mmol) was added to a 20-mL aqueous solution of $[(Me_3tacn)Cr(CN)_3] \cdot H_2O$ (482 mg, 1.60 mmol), resulting in the immediate precipitation of a pale solid, which redissolved after the mixture began to boil. The clear, orange solution was then reduced to 20 mL with heat. After allowing the concentrated solution to reach room temperature, MeCN (35 mL) was added to precipitate the crude product. The orange solid was isolated by filtration and redissolved in 20 mL of $H_2O$. Slow evaporation of the solution yielded 296 mg of orange, microcrystalline powder. Following filtration, the product was washed with 5 mL of MeCN and 5 of mL $Et_2O$. The mother liquor was further concentrated with heat and then allowed to evaporate slowly several times; this produced three additional crops (114, 171, 124 mg), affording a total yield of 705 mg (94%). Anal. Calcd. (%) for $C_{96}H_{222}N_{48}Cr_8Pt_6Cl_{12}O_{27}$: C, 25.66; H, 4.98; N, 14.96. Found: C, 26.19; H, 5.36; N, 14.46. IR: (solid) $\nu_{CN}$ 2208 (w), 2172 (s) $cm^{-1}$; ($H_2O$) $\nu_{CN}$ 2175 $cm^{-1}$; (DMSO) $\nu_{CN}$ 2173 $cm^{-1}$. Absorption spectrum ($H_2O$): $\lambda_{max}$/nm ($\epsilon_M$ /$M^{-1}$ $cm^{-1}$) 223 (171 000), 258 (61 500), 270 (sh), 296 (9190), 358 (442), 467 (560). $ES^+$-MS (2:1 MeOH:$H_2O$): *m*/*z* 1300 ([**1**–27$H_2O$–3Cl]$^{3+}$), 966 ([**1**–27$H_2O$–4Cl]$^{4+}$), 766 ([**1**–27$H_2O$–5Cl]$^{5+}$), 632 ([**1**–27$H_2O$–6Cl]$^{6+}$), 537 ([**1**–27$H_2O$–7Cl]$^{7+}$). Cyclic Voltammogram (1 mM; $[(Bu_4N)BF_4]$ = 0.1 M; dry, de-oxygenated DMSO): $E_{1/2}$ = −1.59 V ($\Delta E_p$ = 211 mV) versus $Cp_2Fe/Cp_2Fe^+$. Orange, parallelepiped-shaped crystals of $[(Me_3tacn)_8Cr_8Pt_6(CN)_{24}]Cl_{12} \cdot 37H_2O$ (**1**·10$H_2O$) suitable for X-ray analysis, were obtained from a slow diffusion of THF into a concentrated aqueous solution of **1**.

*[(Me$_3$tacn)$_8$Cr$_8$Pt$_6$(CN)$_{24}$][Pt(CN)$_4$]$_6$·6H$_2$O (2)*

A 5-mL solution of $K_2[PtCl_4]$ (87 mg, 0.21 mmol) in $H_2O$ was added to a 10-mL aqueous solution of $[(Me_3tacn)Cr(CN)_3] \cdot H_2O$ (110 mg, 0.35 mmol). Heating and stirring the reaction mixture for 1.5 h afforded a clear, orange solution. After allowing the solution to cool to room temperature, a 5-mL aqueous solution of $K_2[Pt(CN)_4]$ (79 mg, 0.21 mmol) was added. The resultant precipitate was filtered and washed with 5 mL of $H_2O$, 2 mL of MeCN, and 2 mL of $Et_2O$. Drying in air gave 140 mg (73%) of product as a peach-colored solid. Anal. Calcd. (%) for $C_{120}H_{180}N_{72}Cr_8Pt_{12}O_6$: C, 26.28; H, 3.31; N, 18.39. Found: C, 26.71; H, 3.67; N, 18.02. IR: (solid) $\nu_{CN}$ 2208 (w), 2172 (s), 2127 (m) $cm^{-1}$; (DMSO) $\nu_{CN}$ 2174 (m), 2123 (w) $cm^{-1}$. Absorption spectrum (DMSO): $\lambda_{max}$/nm ($\epsilon_M$ / $M^{-1}$ $cm^{-1}$) 351 (39 600), 467 (567). Cyclic Voltammogram (1 mM; $[(Bu_4N)BF_4]$ = 0.1 M; dry, deoxygenated DMSO): $E_{1/2}$ = −1.50 V

($\Delta E_p$ = 430 mV) versus $Cp_2Fe/Cp_2Fe^+$. Orange, parallelepiped-shaped crystals of $[(Me_3tacn)_8Cr_8Pt_6(CN)_{24}][Pt(CN)_4]_6 \cdot 35H_2O$ (**2** $\cdot 29H_2O$) suitable for X-ray analysis, were grown by layering 20 mL of $H_2O$ onto a concentrated 1-mL DMSO solution of the product.

*$[(Me_3tacn)_8Mo_8Pt_6(CN)_{24}][Pt(CN)_4]_6 \cdot 46H_2O$ (3)*

$K_2[PtBr_4]$ (14 mg, 0.024 mmol) in 1 mL of water was added to a 1-mL aqueous solution of $[(Me_3tacn)Mo(CN)_3]$ (14 mg, 0.040 mmol), producing a cloudy, brown mixture. More precipitate formed as the reaction mixture was stirred and heated at 60 °C for 3 h. After filtering to remove the orange solid, the brown solution was concentrated by evaporation in air for one week, resulting only in more amorphous powder. Following removal of the solid, the solution was diluted with an additional 4 mL of water and once again concentrated by evaporation in air. Two weeks later, yellow–orange, hexagonal tablets had formed, along with some red-orange, crystalline material. The tablets were suitable for X-ray analysis and were identified as $[(Me_3tacn)_8Mo_8Pt_6(CN)_{24}][Pt(CN)_4]_6 \cdot 46H_2O$ **(3)**. Less than 2 mg of the product mixture could be isolated after crystal selection for X-ray and IR analyses. IR (solid): $\nu_{CN}$ 2185 (w), 2152 (s), 2130 (m) $cm^{-1}$.

*$[(Me_3tacn)_8Mo_8Pt_6(CN)_{24}][Pt(CN)_4]_{2.5}[Pt(CN)_3Br]_2Br_3 \cdot 6H_2O$ (4)*

This compound was isolated from a reaction similar to the preparation for **3**; however, after removal of the second crop of amorphous precipitate, the diluted solution was left untouched and covered for 13 months. The resulting mixture was mainly composed of crystals of **3** and smaller, red–orange, tristruncated trigonal prisms, which X-ray analysis identified as $[(Me_3tacn)_8Mo_8Pt_6(CN)_{24}][Pt(CN)_4]_{2.5}[Pt(CN)_3Br]_2Br_3 \cdot 6H_2O$ (**4**). IR (solid): $\nu_{CN}$ 2183 (w), 2145 (s) $cm^{-1}$.

## X-ray Structure Determinations

Single crystals were coated with Paratone-N oil, attached to glass fibres, transferred to a CCD area-detector diffractometer (Bruker/Nonius SMART or Bruker APEX), and cooled in a dinitrogen stream. Initial lattice parameters were obtained from a least-squares analysis of more than 700 reflections; these parameters were later refined against all data. None of the crystals showed significant decay during data collection. Data were integrated and corrected for Lorentz and polarization effects using SAINT and were empirically corrected for absorption effects using SADABS [12].

Space group assignments were based on systematic absences, $E$ statistics, and successful structural refinement. Structures were solved by direct methods with the aid of successive difference Fourier maps and were refined against all data using the SHELXTL 5.1 software package [13]. As a result of the large number of atoms in $\mathbf{1}\cdot 10H_2O$, later refinement of the model had to be completed in blocks; while the metals were refined in each cycle, the low-$Z$ atoms of the two molecules in the asymmetric unit were refined separately. Thermal parameters for all non-hydrogen atoms in $\mathbf{1}\cdot 10H_2O$, $\mathbf{2}\cdot 29H_2O$, and **4** were refined anisotropically, except for the disordered carbon and nitrogen atoms. It was necessary, however, to restrain the anisotropy of four atoms in the bridging cyanides of $\mathbf{1}\cdot 10H_2O$ and five atoms in the terminal cyanides of $\mathbf{2}\cdot 29H_2O$. In the structure of **3**, only the metals could be refined anisotropically because of the presence of some intense outliers in the diffraction data. Since crystals of this compound tend to form around amorphous or microcrystalline material, it is necessary to cut them to isolate an X-ray quality single-crystal. The outlying data may originate from such material that was not thoroughly removed or from a fragment of the crystal created during the cutting process. Unfortunately, X-ray quality crystals of **3** are not easily grown, so this is in fact the highest resolution data set available. For all structures, the final residual factors are high owing to the extensive disorder in the crystals and the poor quality of the crystals available.

The ethylene bridges of the $Me_3$tacn in all structures are disordered over at least two conformations. Most bridge atoms were modeled with half-occupancy at two sites; however, in order to maintain appropriate connectivity, certain atoms were left fully-occupied, with highly anisotropic thermal ellipsoids. In cases where neither the ordered or simple disordered model refined successfully, bond length restraints were used to stabilize the disordered model. If the softer restraint of setting analogous bond distances to be similar was insufficient, the bond lengths were fixed to be within 0.02 Å of the known distances (obtained by averaging bond lengths in the Cambridge Structural Database – CSD). Such restraints are present in five of the nine $Me_3$tacn ligands in $\mathbf{1}\cdot 10H_2O$.

The bond lengths of the square planar anions of $\mathbf{2}\cdot 29H_2O$, **3,** and **4** were set to be near the mean distances, provided by the CSD. In the structure of **4**, the extensive disorder surrounding the cluster involves high-$Z$ atoms; attempts to obtain a model with a larger unit cell did not simplify the disorder. The two tetracyanoplatinate anions capping the cluster of **4** have half-occupancy; one of them could only be modeled with three cyanides because the fourth is too near the platinum of a symmetry-related anion. The bromide of the capping $[Pt(CN)_3Br]^{2-}$ in **4** is disordered over all four coordination sites; the cyano/bromo ratio of each ligand was allowed to

refine individually. Five sites with high electron density at least 3.2 Å away from the cluster were assigned as four partial bromides and one partial $[Pt(CN)_4]^{2-}$; the latter was modelled as such because it appeared as an aggregate of significant electron density with a strong, central difference Fourier peak. Since its ligand set cannot be precisely located, it has been modelled as partially-occupied oxygen atoms using the approach utilized for the disordered solvent water molecules (*vide infra*). The occupancy of this platinum atom was refined with two neighboring partially-occupied bromides to ensure charge balance.

The solvate water molecules of all structures are highly disordered. Following assignment of all cluster atoms, any strong difference Fourier peaks found non-bonded to the clusters were assigned as oxygen atoms with a fixed isotropic thermal parameter and an occupancy free to refine. The thermal parameter was set to be comparable to the larger values observed in the disordered atoms of the cluster molecules. Difference Fourier peaks were assigned as oxygen atoms until their occupancies refined to less than 0.25 oxygen atoms (i.e. 2 electrons). In $\mathbf{1} \cdot 10H_2O$, the solvate water and the chloride anions cannot be reliably distinguished; consequently, charge balance was achieved by later assigning the highest occupied "oxygen atoms" as chlorine atoms.

Hydrogen atoms associated with the solvate water molecules or the disordered ethylene bridges were not included in the refinement; all other hydrogen atoms were assigned ideal positions. The hydrogen atoms of those methyl groups sitting on a mirror plane in $\mathbf{1} \cdot 10H_2O$ could not be refined, so they were only determined in the final model. The remaining hydrogen atoms were refined using a riding model with an isotropic thermal parameter 1.2 or 1.5 times the attached carbon atom, for methylene and methyl carbons, respectively.

Crystallographic data for the structural analyses have been deposited with the Cambridge Crystallographic Data Centre, CCDC Nos. 638033, 638034, 638035, and 638036 for $\mathbf{1} \cdot 10H_2O$, $\mathbf{2} \cdot 29H_2O$, **3**, and **4**, respectively. Copies of this information may be obtained free of charge from the Director, CCDC, 12 Union Road, Cambridge, CB2 1EZ, UK. [fax: (int.code) +44(1223)-336–033 or e-mail: deposit@ccdc.cam.ac.uk or www: http://www.ccdc.cam.ac.uk].

## Other Physical Measurements

Elemental microanalysis was performed at the Micro-mass facility of the College of Chemistry, UC Berkeley. Infrared spectra were recorded on a Nicolet Avatar 360 FTIR spectrometer equipped with an attenuated-total-

reflectance accessory. Absorption spectra were measured with a Hewlett-Packard 8453 spectrophotometer. Mass spectrometric measurements were performed in the positive-ion mode on a VG Quattro (Micromass) spectrometer or a Bruker Apex II 7T actively shielded FT-ICR mass spectrometer, which were equipped with an analytical electrospray ion source. Electrochemical measurements were conducted with a Bioanalytical Systems CV-50 potentiostat under a dinitrogen atmosphere; platinum disk working, platinum wire auxiliary, and silver wire reference electrodes were used, with $(NBu_4)(BF_4)$ as the supporting electrolyte and ferrocene as an internal reference.

## RESULTS AND DISCUSSION

### Incorporating Platinum into a Face-Centered Cubic Cluster

As in the synthesis of the analogous chromium-nickel face-centered cubic cluster compound [8], $[(Me_3tacn)_8Cr_8Pt_6(CN)_{24}]Cl_{12} \cdot 27H_2O$ (**1**) is prepared by an assembly reaction in boiling aqueous solution:

$$8\left[(Me_3tacn)Cr(CN)_3\right] + 6K_2[PtCl_4] \rightarrow \left[(Me_3tacn)_8Cr_8Pt_6(CN)_{24}\right]Cl_{12} \cdot 27H_2O + 12KCl \quad (3)$$

Better yields of **1**, however, can be obtained with an excess of the chromium reagent, which discourages a competing reaction that produces an unidentified peach solid. The desired product is later separated from the excess $[(Me_3tacn)Cr(CN)_3]$ by precipitation from solution upon addition of acetonitrile, enabling the isolation of compound **1** as an orange solid.

Although the precise identity of the peach precipitate obtained from reaction 3 is unknown, it also reacts with $[(Me_3tacn)Cr(CN)_3]$ in boiling aqueous solution to produce compound **1**. Its insolubility in water and other organic solvents indicates that it is likely an extended metal-cyanide network, which would also be consistent with its higher yields when more of the "unblocked" reagent, $K_2[PtCl_4]$, is present. Furthermore, its infrared spectrum contains a single cyanide stretch ($\nu_{CN} = 2166\ cm^{-1}$) that is higher in energy than that of $[(Me_3tacn)Cr(CN)_3]$ or $K_2[Pt(CN)_4]$, suggesting a bridging cyanide ligand.

Crystallization of **1** is possible by diffusing THF, acetonitrile, or acetone vapor into an aqueous solution, or by simply allowing the aqueous solution to concentrate through evaporation. X-ray analysis of the best single-crystals, obtained using the THF/water system, revealed *C*-centered monoclinic symmetry (Table I) within $[(Me_3tacn)_8Cr_8Pt_6(CN)_{24}]Cl_{12} \cdot 37H_2O$ ($\mathbf{1} \cdot 10H_2O$), as opposed to the rhombohedral crystal systems of the

**Table I.** Crystallographic Data[a] and Refinement Parameters for $[(Me_3tacn)_8Cr_8Pt_6(CN)_{24}]Cl_{12} \cdot 37H_2O$ (**1** · $10H_2O$) and $[(Me_3tacn)_8Cr_8Pt_6(CN)_{24}][Pt(CN)_4]_6 \cdot 35H_2O$ (**2** · $29H_2O$)

| | **1** · $10H_2O$ | **2** · $29H_2O$ |
|---|---|---|
| Formula | $C_{96}H_{242}N_{48}Cr_8Pt_6Cl_{12}O_{37}$ | $C_{120}H_{238}N_{72}Cr_8Pt_{12}O_{35}$ |
| Formula weight | 4673.32 | 6006.90 |
| Temperature, K | 144 | 155 |
| Crystal size, mm | $0.22 \times 0.15 \times 0.12$ | $0.32 \times 0.26 \times 0.22$ |
| Crystal system | Monoclinic | Monoclinic |
| Space group | $C2/m$ | $P2_1/n$ |
| $a$, Å | 63.0711 (11) | 18.7004 (5) |
| $b$, Å | 28.6311 (6) | 18.9159 (5) |
| $c$, Å | 17.8610 (4) | 32.0611 (6) |
| β, deg | 96.735 (1) | 101.031 (1) |
| Volume, Å$^3$ | 32030.7 (11) | 11131.6 (5) |
| $Z$ | 6 | 2 |
| $D_c$, g cm$^{-3}$ | 1.408 | 1.736 |
| Absorption coefficient, mm$^{-1}$ | 4.514 | 7.947 |
| $R_{int}$ | 0.0918 | 0.0836 |
| Data/restraints/parameters | 19324/52/1476 | 14917/66/1099 |
| Goodness-of-fit on $F^2$ | 1.024 | 1.022 |
| $R_1$, w$R_2$ [b] | 0.0876, 0.2498 | 0.0745, 0.1986 |

[a] Obtained with graphite monochromated Mo Kα (λ = 0.7103 Å) radiation.
[b] $R_1 = T||F_o| - |F_c||/T|F_o|$, $wR_2 = \{ T [w(F_o^2 - F_c^2)^2]/T[w(F_o^2)^2]\}^{1/2}$.

analogous nickel-containing species [8a, 9]. Nevertheless, the clusters within **1** · $10H_2O$ exhibit the usual face-centered cubic structure, wherein eight $Cr^{III}$ centers are situated at the corners of a cube with six platinum ions lying just above the center of each face (see Fig. 1). The metal ions are connected via cyanide bridges that have undergone a thermally-induced linkage isomerization resulting in a $Pt^{II}$–C ≡ N–$Cr^{III}$ connectivity. A similar process has been documented in the $M_8Ni_6$ (M = Cr [8a], Mo [9]) analogues and other cyanometalate systems [14]; it arises from the preference of the softer carbon-end of cyanide for the softer metal ion (in this case, $Pt^{II}$ rather than $Cr^{III}$). As a result, the $Pt^{II}$ centers have four cyanide ligands ensuring their square planar geometry, while the $Cr^{III}$ centers maintain their octahedral geometry with the blocking ligand bound facially and the nitrogen-end of three cyanides in the remaining coordination sites. Solvent is not observed within the internal cavity of the cluster; in the case of water, this is likely due to the hydrophobic nature of the cluster interior [8a]. The absence of included solvent is confirmed by the electrospray mass spectrum, which also confirms the presence of the intact cluster in solution (see Fig. 2).

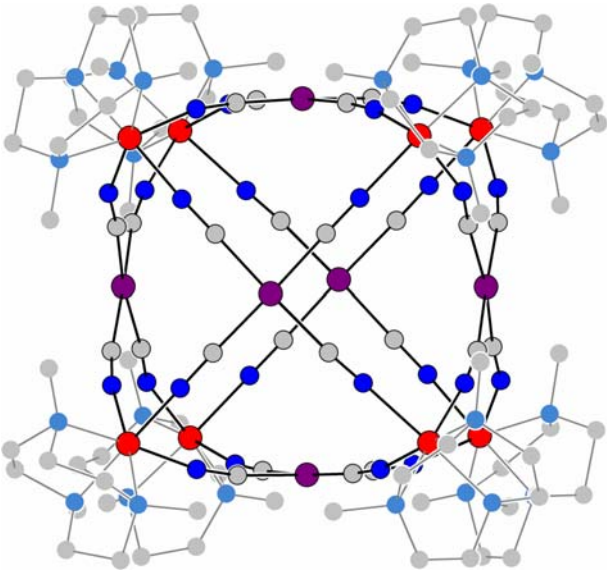

**Fig. 1** Structure of the face-centered cubic cluster $[(Me_3tacn)_8Cr_8Pt_6(CN)_{24}]^{12+}$, as observed in the molecule that resides on the 2/*m* symmetry site of $\mathbf{1}\cdot 10H_2O$. Purple, red, grey, and blue spheres represent Pt, Cr, C, and N atoms, respectively; H atoms are omitted for clarity. The disordered $Me_3tacn$ ligands are shown in only one of their conformations and have been faded for better visualization of the cluster core. The other molecule in the asymmetric unit resides on a mirror plane.

The asymmetric unit in $\mathbf{1}\cdot 10H_2O$ contains fragments from two independent molecules; one $Cr_8Pt_6$ cluster lies on a mirror plane that bisects the cube diagonally (molecule A), while the other is centered on a 2/*m* symmetry site (molecule B). Although the metal-cyanide frame can be idealized as having $O_h$ point symmetry, closer inspection of the metal···metal separations reveal that a pair of Cr···Cr distances defining opposite edges of the cube are shorter than the other edge distances by 0.1 and 0.2 Å for molecules A and B, respectively. The more significant edge shortening in molecule B is accompanied by a contraction of the parallel *trans*-Pt···Pt distance by more than 0.1 Å. These deviations from ideal octahedral symmetry appear to originate from the crystal packing and are consistent with the lower symmetry of the crystal system of $\mathbf{1}\cdot 10H_2O$.

The incorporation of a 5*d* transition metal into the face-centered cubic framework leads to a larger cluster relative to the first-row analogue $[(Me_3tacn)_8Cr_8Ni_6(CN)_{24}]^{12+}$ [8a]. Table II provides a list of mean interatomic distances and angles of both clusters, for comparison. As expected, accommodation of $Pt^{II}$ at the face-centering sites pushes the $Cr^{III}$ centers

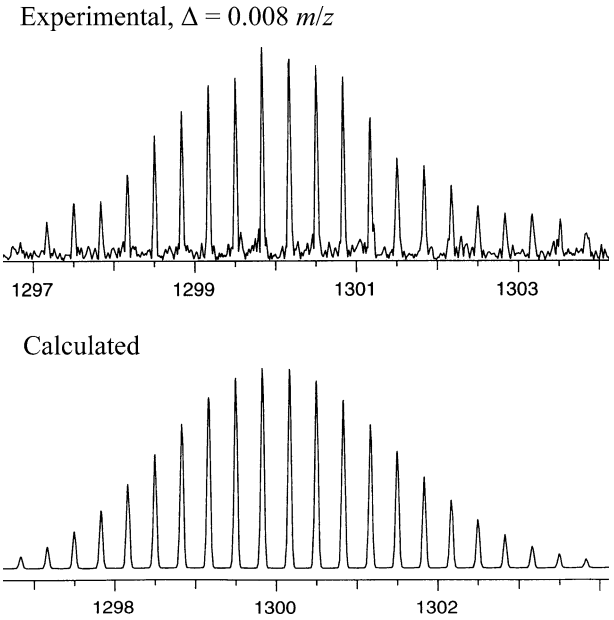


**Fig. 2** Portion of the electrospray mass spectrum indicating the presence of $\{[(Me_3\text{-}tacn)_8Cr_8Pt_6(CN)_{24}]Cl_9\}^{3+}$ in a 0.5 mM solution of compound **1** in MeOH:$H_2O$ (2:1), along with the calculated isotope pattern.

further away from each other, lengthening the mean cube edges from 6.97(2) to 7.208(2) Å. Conversely, the *trans*-Pt···Pt distance decreases. Considering the van der Waals radius of platinum (1.72 Å) [15], this results in a minimum diameter of 5.4 Å for the inner cavity of the $Cr_8Pt_6$ cluster, which, surprisingly, is smaller than that of the $Cr_8Ni_6$ cluster (5.6 Å) [8a]. Furthermore, the $[Pt(CN)_4]^{2-}$ units on the cube faces are more planar, with the $Pt^{II}$ centers residing only 0.8067(1) Å beyond the $Cr_4$ planes, whereas the nickel ions are pushed 0.934(3) Å outwards in the $Cr_8Ni_6$ cluster [8a]. Presumably, this effect is associated with the better overlap between the 5*d* orbitals of platinum and the cyanide C orbitals, which leads to *trans*-C–Pt–C bond angles that are nearer to 180°. The flattening of the $[M'(CN)_4]^{2-}$ units may also account for why the $Pt^{II}$ centers do not exhibit any evident axial interactions with the halide anions or solvating water, as observed for all of the nickel-containing cluster analogues [7a, 8a, 9].

Although we do not know the precise structure of compound **1** in solution, the cluster is at least to some extent intact, as indicated by the electrospray mass spectrum (see Fig. 2) and by infrared spectroscopy. The

**Table II.** Selected Mean Interatomic Distances (Å) and Angles (deg) for Face-Centered Cubic $[(Me_3tacn)_8Cr_8M'_6(CN)_{24}]^{12+}$ (M′ = Ni, Pt) Clusters in the Structures of $[(Me_3tacn)_8Cr_8Ni_6(CN)_{24}]Br_{12}\cdot 45H_2O$ [8a], $[(Me_3tacn)_8Cr_8Pt_6(CN)_{24}]Cl_{12}\cdot 37H_2O$ ($\mathbf{1}\cdot 10H_2O$), and $[(Me_3tacn)_8Cr_8Pt_6(CN)_{24}][Pt(CN)_4]_6\cdot 35H_2O$ ($\mathbf{2}\cdot 29H_2O$)[a]

| | M′ = Ni | $\mathbf{1}\cdot 10H_2O$ | $\mathbf{2}\cdot 29H_2O$ |
|---|---|---|---|
| Cr···Cr | 6.97 (2) | 7.208 (2) | 7.164 (2) |
| *trans*-M′···M′ | 8.844 | 8.8115 (8) | 8.7042 (9) |
| min. diameter, inner cavity[b] | 5.6 | 5.4 | 5.3 |
| M′···cube face ($Cr_4$ plane) | 0.934 (3) | 0.8067 (1) | 0.7705 (1) |
| Pt–Pt | | | 3.1552 (7) |
| M′–C | 1.873 (9) | 1.999 (5) | 1.997 (6) |
| C–$N_{CN}$ | 1.145 (6) | 1.134 (6) | 1.118 (6) |
| Cr–$N_{CN}$ | 2.031 (7) | 2.067 (5) | 2.053 (6) |
| Cr–$N_{tacn}$ | 2.066 (6) | 2.057 (4) | 2.066 (6) |
| C–M′–C | 89.6 (3) | 90.0 (1) | 90.0 (3) |
| | 170.0 (5) | 175.8 (3) | 176.0 (3) |
| M′–C–$N_{CN}$ | 177 (2) | 174.1 (5) | 176.7 (6) |
| Cr–$N_{CN}$–C | 169.1 (5) | 167.4 (4) | 166.8 (5) |
| $N_{CN}$–Cr–$N_{CN}$ | 88.0 (3) | 88.0 (1) | 87.2 (2) |
| $N_{tacn}$–Cr–$N_{tacn}$ | 83.0 (1) | 83.8 (2) | 83.7 (3) |

[a] $N_{CN}$ and $N_{tacn}$ indicate N atoms in cyanide and $Me_3tacn$ ligands, respectively.
[b] Calculated by subtracting the van der Waals radii of M′ [15] from the *trans*-M′···M′ separation.

cyclic voltammogram of **1** in DMSO exhibits a partially reversible reduction event centered at $E_{1/2} = -1.59$ V versus the $Fe^{II}/Fe^{III}$ couple of ferrocene. Unfortunately, however, attempts to isolate the reduced product via bulk chemical reduction resulted only in decomposition products.

## Capping the Cluster Faces with $[Pt(CN)_4]^{2-}$

The $Cr_8Ni_6$ face-centered cubic cluster is known to form the neutral aggregate species $[(Me_3tacn)_8Cr_8Ni_6(CN)_{24}][Ni(CN)_4]_6$, in which each of the face-centering nickel atoms has an axial contact with the nickel atom of a face-capping tetracyanonickelate counteranion [8a]. The metal–metal interaction arises from the admixing of the empty $p_z$ orbitals and the filled $d_z^2$ orbitals of the $Ni^{II}$ centers. The chromium–platinum analogue was anticipated to be a promising precursor to a high-spin cluster because its Pt–Pt interactions were likely to be comparable to those observed in simple tetracyanoplatinates. Many salts of $[Pt(CN)_4]^{2-}$ can be oxidized to produce *quasi*-one-dimensional conductive chains, formally containing both divalent

and trivalent platinum ions [16]. If the neutral chromium–platinum aggregate could be similarly oxidized, the mixed-valency among the platinum ions in the resulting species could possibly induce the exchange coupling necessary to produce a high-spin molecule.

The preparation of the chromium–platinum capped aggregate parallels that of the chromium–nickel system [8a]. In a simple aqueous ion-exchange reaction, the twelve chloride anions of compound **1** are replaced with six $[Pt(CN)_4]^{2-}$ anions, affording $[(Me_3tacn)_8Cr_8Pt_6(CN)_{24}][Pt(CN)_4]_6 \cdot 6H_2O$ (**2**):

$$\begin{aligned}&\left[(Me_3tacn)_8Cr_8Pt_6(CN)_{24}\right]Cl_{12} \;+\; 6K_2\left[Pt(CN)_4\right] \rightarrow \\ &\left[(Me_3tacn)_8Cr_8Pt_6(CN)_{24}\right]\left[Pt(CN)_4\right]_6 \;+\; 12KCl\end{aligned} \tag{4}$$

The product is completely insoluble in water, allowing for a clean reaction even when **1** is in solution with the excess $[(Me_3tacn)Cr(CN)_3]$ used for its synthesis. Furthermore, when fewer than six equivalents of $[Pt(CN)_4]^{2-}$ are employed, so as to target the cubic cluster with chloride *and* tetracyanoplatinate anions, **2** remains the only precipitate.

Despite its insolubility in water and most common organic solvents, compound **2** can be dissolved in DMSO. Carefully layering the solution with water eventually produced X-ray quality crystals of $[(Me_3tacn)_8Cr_8Pt_6(CN)_{24}][Pt(CN)_4]_6 \cdot 35H_2O$ (**2** $\cdot 29H_2O$) in the monoclinic space group, $P2_1/n$ (see Table I). The structure of **2**$\cdot 29H_2O$ is isomorphous to the neutral $Cr_8Ni_{12}$ aggregate [8a], but its unit cell is approximately 450 Å$^3$ larger to accommodate the 5*d* metal ions. The one molecule in the asymmetric unit resides on an inversion center. As is evident in Fig. 3, this molecule is indeed the $Cr_8Pt_6$ cluster observed in **1** $\cdot 10H_2O$, but with a tetracyanoplatinate anion capping each cube face. The capping $[Pt(CN)_4]^{2-}$ units are arranged in a staggered fashion, with a mean Pt–Pt contact of 3.1552(7) Å, a value within the range observed in simple tetracyanoplatinate salts [16]. The $[Pt(CN)_4]^{2-}$ units within the $Cr_8Pt_6$ cluster are even closer to planarity than in the uncapped precursor; this flattening effect of the capping process was also observed in the analogous chromium–nickel system [8a]. With the face-centering platinum ions residing only 0.7705(1) Å above the cube faces, the internal cavity of the capped $Cr_8Pt_{12}$ cluster is the smallest observed among the $[(Me_3tacn)_8M_8M'_6(CN)_{24}]^{12+}$ clusters. No other significant differences are apparent in comparing the $Cr_8Pt_6$ cages within **1** $\cdot 10H_2O$ and **2** $\cdot 29H_2O$, but the individual metal···metal distances in the scaffold of the capped $Cr_8Pt_{12}$ species are more congruent. As a result, ignoring the various conformations of $Me_3tacn$, the neutral, capped cluster is closer to $O_h$ symmetry than its cationic precursor.

In solution, the $Cr_8Pt_6$ cluster of compound **2** also appears to be intact, as suggested by the infrared spectrum of its DMSO solution. Unfortunately,

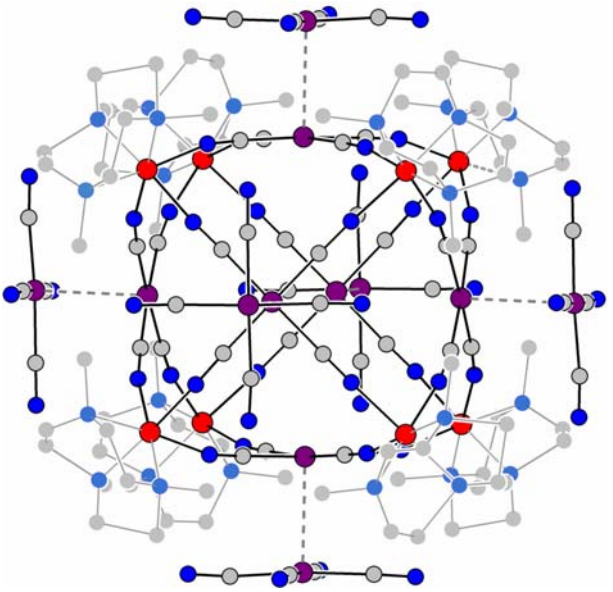

**Fig. 3** Structure of the capped face-centered cubic cluster $[(Me_3tacn)_8Cr_8Pt_6(CN)_{24}][Pt(CN)_4]_6$, as observed in $\mathbf{2}\cdot 29H_2O$. Purple, red, grey, and blue spheres represent Pt, Cr, C, and N atoms, respectively; H atoms are omitted for clarity. The disordered $Me_3tacn$ ligands are shown in only one of their conformations and have been faded for better visualization of the cluster core and the capping anions. The molecule resides on an inversion center within the crystal structure. The cluster in **3** is isomorphous.

the interactions with the capping anions are disrupted; the stretching frequency of the terminal cyanide ligands shifts slightly from 2130 to 2123 $cm^{-1}$, which is identical to the frequency observed for a DMSO solution of $K_2[Pt(CN)_4]$. In addition, the cyclic voltammogram of compound **2** is very similar to that of compound **1**. Thus, it is unlikely that an oxidation similar to those in unsupported tetracyanoplatinates could be realised through solution chemistry.

## Targeting $Mo_8Pt_6$ Clusters

As mentioned previously, the intriguing electrochemistry observed for the $[(Me_3tacn)_8Mo_8Ni_6(CN)_{24}]^{12+}$ cluster prompted us to pursue an analogous platinum-containing species. Accordingly, numerous attempts were made to extend reaction 3 to accommodate use of $[(Me_3tacn)Mo(CN)_3]$. In addition, $K_2[PtBr_4]$ was tried as the platinum reagent, in

hopes of having better resolved anions in the crystal structure. An analogous reaction certainly occurs:

$$\begin{aligned} &8\left[(Me_3tacn)Mo(CN)_3\right] + 6[PtBr_4]^{2-} \rightarrow \\ &\left[(Me_3tacn)_8Mo_8Pt_6(CN)_{24}\right]^{12+} + 24Br^- \end{aligned} \tag{5}$$

In the presence of platinum, however, the cyanide ligands of $[(Me_3tacn)Mo(CN)_3]$ are apparently very labile. Some of the bromide anions of the tetrabromoplatinates are subsequently replaced by cyanides, and the ensuing cyanoplatinates precipitate a variety of capped, face-centered cubic cluster compounds:

$$\begin{aligned} &\left[(Me_3tacn)_8Mo_8Pt_6(CN)_{24}\right]^{12+} + n\left[Pt(CN)_{(4-x)}Br_x\right]^{2-} \\ &\quad + mBr^-\,(x = 0-1,\ 2n + m = 12) \rightarrow \\ &\qquad \left[(Me_3tacn)_8Mo_8Pt_6(CN)_{24}\right]\left[Pt(CN)_4\right]_6 \cdot 46H_2O + \\ &\qquad \left[(Me_3tacn)_8Mo_8Pt_6(CN)_{24}\right]\left[(Pt)(CN)_4\right]_{2.5} \\ &\qquad [Pt(CN)Br_3]_2Br_3 \cdot 6H_2O + \cdots \end{aligned} \tag{6}$$

Although the identity of all products is not known, the fully-capped and a partially-capped species were successfully characterized crystallographically (see Table III). Yellow–orange, hexagonal tablet-shaped crystals were identified as containing the capped cluster compound $[(Me_3tacn)_8Mo_8Pt_6(CN)_{24}][Pt(CN)_4]_6 \cdot 46H_2O$ (**3**). Despite the limited structural refinement, its identity is clear as it has a unit cell isomorphous to that of $\mathbf{2} \cdot 29H_2O$. Furthermore, its infrared spectrum has a similar pattern of cyanide stretches: the two higher-energy stretches at $\nu_{CN} = 2185$ and 2152 $cm^{-1}$ can be attributed to the bridging cyanides, while the lower-energy stretch at $\nu_{CN} = 2130$ $cm^{-1}$, can be assigned to the terminal cyanides of the capping tetracyanoplatinate anions.

Dispersed among the crystals of compound **3** were tiny red–orange rod-shaped crystals of a related compound. Crystals of this second product suitable for X-ray analysis were only obtained after a reaction solution was left untouched for thirteen months. They were then identified as the partially-capped cluster compound $[(Me_3tacn)_8Mo_8Pt_6(CN)_{24}][Pt(CN)_4]_{2.5}[Pt(CN)_3Br]_2Br_3 \cdot 6H_2O$ (**4**), which crystallizes in the same monoclinic space group, $P2_1/n$, as the fully-capped cluster. While the $Mo_8Pt_6$ cage and the two $[Pt(CN)_3Br]^{2-}$ anions are evident in the crystal structure, a large amount of disorder exists among the other metal-containing anions. Three independent tetracyanoplatinate faces exist in the central cluster, such that opposite faces of the cube are related to one another by inversion symmetry. Capping one

**Table III.** Crystallographic Data[a] and Refinement Parameters for $[(Me_3tacn)_8Mo_8Pt_6(CN)_{24}][Pt(CN)_4]_6 \cdot 46H_2O$ (**3**) and $[(Me_3tacn)_8Mo_8Pt_6(CN)_{24}][Pt(CN)_4]_{2.5}[Pt(CN)_3Br]_2Br_3 \cdot 6H_2O$ (**4**)

| | **3** | **4** |
|---|---|---|
| Formula | $C_{120}H_{260}N_{72}Mo_8Pt_{12}O_{46}$ | $C_{112}H_{180}N_{64}Mo_8Pt_{10.5}Br_5O_6$ |
| Formula weight | 6556.60 | 5734.71 |
| Temperature, K | 160 | 155 |
| Crystal size, mm | $0.20 \times 0.11 \times 0.08$ | $0.12 \times 0.04 \times 0.04$ |
| Crystal system | Monoclinic | Monoclinic |
| Space group | $P2_1/n$ | $P2_1/n$ |
| $a$, Å | 18.875 (8) | 19.3671 (12) |
| $b$, Å | 19.130 (8) | 16.5969 (11) |
| $c$, Å | 32.667 (14) | 28.0756 (18) |
| β, deg | 102.218 (12) | 92.9490 (10) |
| Volume, Å$^3$ | 11528 (8) | 9013 (1) |
| $Z$ | 2 | 2 |
| $D_c$, g cm$^{-3}$ | 1.806 | 2.150 |
| Absorption coeeficient, mm$^{-1}$ | 7.738 | 9.814 |
| $R_{int}$ | 0.0868 | 0.0586 |
| Data/restraints/parameters | 13752/36/699 | 11125/33/958 |
| Goodness-of-fit on $F^2$ | 1.009 | 1.177 |
| $R_1$, w$R_2$ [b] | 0.0619, 0.1524 | 0.0633, 0.1646 |

[a] Obtained with graphite monochromated Mo Kα (λ = 0.7103 Å) radiation.
[b] $R_1 = T||F_o| - |F_c||/T|F_o|$, $wR_2 = \{T[w(F_o^2 - F_c^2)^2]/T[w(F_o^2)^2]\}^{1/2}$.

pair of converse faces of the cluster are the two fully-occupied $[Pt(CN)_3Br]^{2-}$ anions arranged in a staggered fashion with a Pt–Pt distance much like those observed in $\mathbf{2} \cdot 29H_2O$ and **3** (see Tables II and IV). The bromide ligand of the anion is disordered over all four ligand sites. Although we are unaware of any reports of halide-cyanide disorder within square planar platinate anions, it has been observed in other systems [17, 18]. At both the second and third types of faces, a $[Pt(CN)_4]^{2-}$ anion is disordered over two positions above opposing faces of the cube. While within the range observed for simple tetracyanoplatinate salts, the axial Pt–Pt contact at the second pair of faces is longer (3.247(2) Å) than those in the fully-capped clusters. Although modeled as $[Pt(CN)_4]^{2-}$, this anion is likely a highly disordered $[Pt(CN)_{4-x}Br_x]^{2-}$ where $1 < x < 4$, because it appears as a relatively planar collection of closely spaced difference Fourier peaks without any evident staggering relative to the tetracyanoplatinate face of the cluster core. The capping anion of the third set of opposing faces is positioned close and staggered as in the fully-capped clusters. Its disorder can alternatively be described as being over two adjoining sites that cap neighboring clusters. One of the cyanide ligands of the anion resides almost directly above the

**Table IV.** Selected Mean Interatomic Distances (Å) and Angles (deg) for Face-Centered Cubic $[(Me_3tacn)_8Mo_8M'_6(CN)_{24}]^{12+}$ (M′ = Ni, Pt) Clusters in the Structures of $[(Me_3tacn)_8Mo_8Ni_6(CN)_{24}]Br_{12}\cdot 30H_2O$ [9], $[(Me_3tacn)_8Mo_8Pt_6(CN)_{24}][Pt(CN)_4]_6\cdot 46H_2O$ (**3**)[a], and $[(Me_3tacn)_8Mo_8Pt_6(CN)_{24}][Pt(CN)_4]_{2.5}[Pt(CN)_3Br]_2Br_3\cdot 6H_2O$ (**4**)[b]

| | M′ = Ni | **3** | **4** |
|---|---|---|---|
| Mo···Mo | 7.07 (5) | 7.269 (1) | 7.250 (1) |
| *trans*-M′···M′ | 9.177 | 8.917 (2) | 9.040 (9) |
| min. diameter, inner cavity[c] | 5.9 | 5.5 | 5.6 |
| M′···cube face ($Mo_4$ plane) | 1.0524 (1) | 0.8204 (2) | 0.8952 (1) |
| Pt–Pt | | 3.1061 (9) | 3.1589 (9) |
| M′–C | 1.86 (1) | 1.994 (2) | 1.982 (6) |
| C–$N_{CN}$ | 1.15 (2) | 1.140 (6) | 1.1139 (6) |
| Mo–$N_{CN}$ | 2.126 (6) | 2.122 (4) | 2.120 (5) |
| Mo–$N_{tacn}$ | 2.175 (8) | 2.175 (5) | 2.184 (5) |
| C–M′–C | 89.5 (4) | 89.2 (2) | 89.8 (2) |
| | 168.6 (1) | 175.8 (3) | 174.0 (3) |
| M′–C–$N_{CN}$ | 176.1 (9) | 175.3 (5) | 175.7 (5) |
| Mo–$N_{CN}$–C | 170.6 (8) | 168.5 (4) | 168.8 (5) |
| $N_{CN}$–Mo–$N_{CN}$ | 88.3 (3) | 87.0 (2) | 87.7 (2) |
| $N_{tacn}$–Mo–$N_{tacn}$ | 80.4 (2) | 80.4 (2) | 81.0 (2) |

[a] Note that the distances for **3** may not be very accurate as the lighter atoms could not be refined anisotropically in the crystal structure.
[b] $N_{CN}$ and $N_{tacn}$ indicate N atoms in cyanide and $Me_3tacn$ ligands, respectively.
[c] Calculated by subtracting the van der Waals radii of M′ [15] from the *trans*-M′···M′ separation.

platinum position of the other symmetry-related, half-occupied site; consequently, the fourth cyanide could not be included in the model. While other int*er*cluster Pt···Pt separations in **4** and all of those in **3** are at least 11 Å, this anion caps platinum atoms of adjacent $Mo_8Pt_6$ clusters that are only 7.74 Å apart (see Fig. 4). The reduced cluster separation is, appropriately, along the *b* axis, the shortest cell dimension of **4**. Along with the fewer tetracyanoplatinate anions present, the denser packing arrangement of the clusters account for why the cell volume of **4** is ca. 2500 $Å^3$ smaller than that of **3**. Charge balance of the partially-capped cluster is achieved by three bromide anions and an additional tetracyanoplatinate anion that do not have any evident interactions with the cluster. The infrared spectrum of compound **4** contains only the two higher energy cyanide stretches, 2183 and 2145 $cm^{-1}$, corresponding to the core cluster; the absence of well-defined terminal cyanides stretches ($\nu$(CN) = 2122 $cm^{-1}$ for $[Pt(CN)_4]^{2-}$) is perhaps consistent with the extensive tetracyanoplatinate disorder present in the crystal structure.

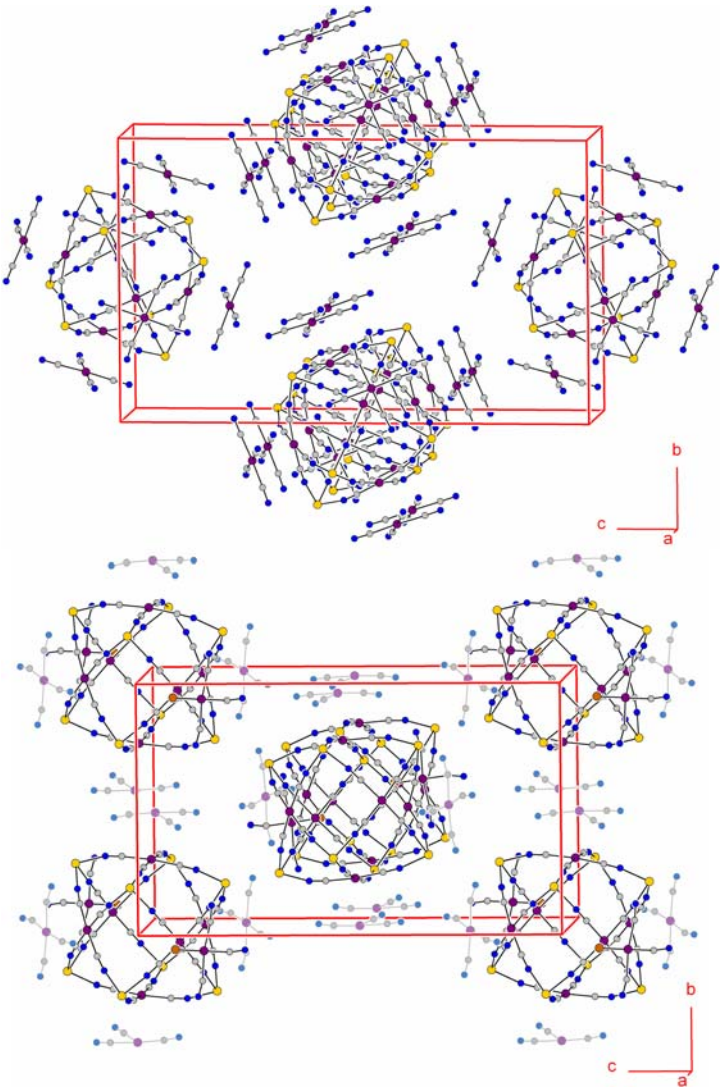


**Fig. 4** Unit cells of the fully-capped (upper) and partially-capped (lower) $Mo_8Pt_6$ face-centered cubic clusters, in **3** and **4**, respectively. Purple, yellow, brown, grey, and blue spheres represent Pt, Mo, Br, C, and N atoms, respectively. The $Me_3$tacn ligands, solvent molecules, and anions without any close contacts to the cluster have been omitted for clarity. All transparent capping anions indicate $[Pt(CN)_4]^{2-}$ with an occupancy of 0.5; the fourth cyanide ligand of one anion could not be modeled due to its proximity to the Pt atom of another partially-occupied tetracyanoplatinate anion.

Despite the limited refinement of **3**, the heavy metal locations should be reliable, permitting comparisons between the different $M_8Pt_6$ cages (see Tables II and IV). As expected, the $Mo_8Pt_6$ cages of **3** exhibit slightly longer metal···metal distances than those of the fully-capped chromium-containing analogue in $\mathbf{2}\cdot 29H_2O$. Contrary to the effect of incorporating heavier metals at the face-centering sites, replacing $Cr^{III}$ with $Mo^{III}$ at the corner sites appears to encourage the $[Pt(CN)_4]^{2-}$ units to bow outwards; this trend was also observed in the analogous $M_8Ni_6$ systems [8a, 9]. Additionally, although an uncapped molybdenum-platinum cube is unavailable for comparison, the trend of flattening tetracyanoplatinate faces is again observed in going from the partially- to the fully-capped species.

In addition to compounds **3** and **4**, reaction 5 also produced amorphous orange powders. The infrared spectra of these products, both crystalline and amorphous, are essentially identical, differing only in the cyanide region. Different batches of the orange powder exhibited cyanide stretches similar to those of **3** or **4**, but elemental analyses never confirmed their identities. Supposing some of these solids were analogous to the peach-colored side-product obtained in the synthesis of **1**, attempts to react them with excess $[(Me_3tacn)Mo(CN)_3]$ were also carried out, but without success. The various powders are likely mixtures of different capped clusters and extended networks; considering the similar fingerprint regions in the infrared spectra of all products, any extended solids present probably contain $(Me_3tacn)Mo\{(CN)–Pt\}_3$ units with bond distances and angles comparable to those observed in **3** and **4**. Unfortunately, all products were highly insoluble, preventing further purification or characterization.

A wide variety of reaction conditions were investigated in targeting an uncapped $Mo_8Pt_6$ cluster product. When $K_2[PtCl_4]$ was used as the platinum reagent in direct parallel with reaction 3, similar mixtures of highly insoluble, amorphous solids were produced. Reactions carried out at room temperature, in hope of avoiding labilization of the cyanide ligands, were equally unsuccessful. In this system, the expected linkage isomerization evidently produces a much more labile cluster species, leading to release of precipitating anions and preventing the isolation of products that can then be further manipulated. Consequently, electrochemical measurements could not be carried out to determine if stepwise reduction of the $Mo^{III}$ centers within a $[(Me_3tacn)_8Mo_8Pt_6(CN)_{24}]^{12+}$ cluster is possible.

## Outlook

With the four new compounds reported here, the face-centered cubic metal-cyanide framework has been successfully extended to include incorporation of $Pt^{II}$ centers at the face-centering sites, reaffirming its versatility.

These species have permitted both synthetic and crystallographic comparisons. While electrochemical characterization of the $Cr_8Pt_6$ cluster has shown that introduction of platinum alone cannot stabilize mixed valence oxidation states of the cluster, incorporating molybdenum as well as platinum into the cluster leads only to insoluble capped cluster products formed upon partial dissociation of cyanide from $[(Me_3tacn)Mo(CN)_3]$. An obvious next step is to pursue the palladium-containing cluster $[(Me_3tacn)_8Mo_8Pd_6(CN)_{24}]^{12+}$, wherein the propensity for subsequent cluster decomposition may lie somewhere in between that of its nickel- and platinum-containing analogues. Indeed, some initial compounds featuring this species have already been isolated [18], and will hopefully enable access to high-spin forms of the face-centered cubic $[(Me_3tacn)_8Mo_8M'_6(CN)_{24}]^{12+}$ clusters via reduction.

## ACKNOWLEDGEMENTS

This work was funded by NSF Grant No. CHE-0617063. NSERC (Canada) and NSF are gratefully acknowledged for providing fellowships to L. M. C. B. and J. J. S., respectively. We thank Dr. C. Crawford and Unilever for the donation of $Me_3tacn$, Dr. M. P. Shores for technical assistance, and Drs. F. J. Hollander and A. G. Oliver for many helpful discussions.

## REFERENCES

1. (a) D. A. Garanin and E. M. Chudnovsky (1997). *Phys. Rev. B.* **56**, 11102. (b) F. Torres, J. M. Hernandez, X. Bohigas, and J. Tejada (2000). *App. Phys. Lett.* **77**, 3248. (c) M. N. Leuenberger and D. Loss (2001). *Nature* **410**, 789. (d) M.-H. Jo, J. E. Grose, K. Baheti, M. M. Deshmukh, J. J. Sokol, E. M. Rumberger, D. N. Hendrickson, J. R. Long, H. Park, and D. C. Ralph (2006). *Nano Lett.* **6**, 2014.
2. C. J. Milios, A. Vinslava, W. Wernsdorfer, S. Moggach, S. Parsons, S. P. Perlepes, G. Christou, and E. K. Brechin (2007). *J. Am. Chem. Soc.* **129**, 2754.
3. (a) R. Sessoli, D. Gatteschi, A. Caneschi, and M. A. Novak (1993). *Nature* **365**, 141. (b) R. Sessoli, H.-L. Tsai, A. R. Schake, S. Wang, J. B. Vincent, K. Folting, D. Gatteschi, G. Christou, and D. N. Hendrickson (1993). *J. Am. Chem. Soc.* **115**, 1804.
4. (a) A. L. Barrar, P. Debrunner, D. Gatteschi, C. E. Schulz, and R. Sessoli (1996). *Europhys. Lett.* **35**, 133. (b) S. L. Castro, Z. Sun, C. M. Grant, J. C. Bollinger, D. N. Hendrickson, and G. Christou (1998). *J. Am. Chem. Soc.* **120**, 2365. (c) A. L. Barrar, A. Caneschi, A. Cornia, B. F. Fabrizi, D. Gatteschi, C. Sangregorio, R. Sessoli, and L. Sorace (1999). *J. Am. Chem. Soc.* **121**, 5302. (d) C. Boskovic, M. Pink, J. C. Huffman, D. N. Hendrickson, and G. Christou (2001). *J. Am. Chem. Soc.* **123**, 9914. (e) C. Boskovic, E. K. Brechin, W. E. Streib, K. Folting, J. C. Bollinger, D. N. Hendrickson, and G. Christou (2002). *J. Am. Chem. Soc.* **124**, 3725. (f) A. J. Tasiopoulos, W. Wernsdorfer, B. Moulton, M. J. Zaworotko, and G. Christou (2003). *J. Am. Chem. Soc.* **125**, 15274. (g) H. Oshio, N. Hoshino, T. Ito, and M.

Nakano (2004). *J. Am. Chem. Soc.* **126**, 8805. (h) E. Coronado, A. Forment-Aliaga, A. Gaita-Ariño, C. Giménez-Saiz, F. M. Romero, and W. Wernsdorfer (2004). *Angew. Chem., Int. Ed.* **43**, 6152. (i) G. Rajaraman, M. Murugesu, E. C. Sañudo, M. Soler, W. Wernsdorfer, M. Helliwell, C. Muryn, J. Raftery, S. J. Teat, G. Christou, and E. K. Brechin (2004). *J. Am. Chem. Soc.* **126**, 15445. (j) S. Maheswaran, G. Chastanet, S. J. Teat, T. Mallah, R. Sessoli, W. Wernsdorfer, and R. E. P. Winpenny (2005). *Angew. Chem., Int. Ed.* **44**, 5044. (k) A. M. Ako, V. Mereacre, I. J. Hewitt, R Clérac, L. Lecren, C. E. Anson, and A. K. Powell (2006). *J. Mater. Chem.* **16**, 2579.

5. (a) T. Mallah, C. Auberger, M. Verdaguer, and P. Veillet (1995). *J. Chem. Soc., Chem. Commun.* 61. (b) A. Scuiller, T. Mallah, M. Verdaguer, A. Nivorzkhin, J.-L. Tholence, and P. Veillet (1996). *New J. Chem.* **20**, 1. (c) K. Van Langenberg, S. R. Batten, K. J. Berry, D. C. R. Hockless, B. Moubaraki, and K. S. Murray (1997). *Inorg. Chem.* **36**, 5006. (d) Z. J. Zhong, H. Seino, Y. Mizobe, M. Hidai, A. Fujishima, S. Ohkoshi, and K. Hashimoto (2000). *J. Am. Chem. Soc.* **122**, 2952. (e) J. Larionova, M. Gross, M. Pilkington, H. Andres, H. Stoeckli-Evans, H.-U. Güdel, and S. Decurtins (2000). *Angew. Chem., Int. Ed.* **39**, 1605. (f) J. J. Sokol, A. G. Hee, and J. R. Long (2002). *J. Am. Chem. Soc.* **124**, 7656. (g) C. P. Berlinguette, D. Vaughn, C. Cañada-Vilalta, J. R. Galán-Mascarós, and K. R. Dunbar (2003). *Angew. Chem., Int. Ed.* **42**, 1523. (h) L. M. C. Beltran and J. R. Long (2005). *Acc. Chem. Res.* **38**, 325 and references therein. (i) M. Ferbinteanu, H. Miyasaka, W. Wernsdorfer, K. Nakata, K. Sugiura, M. Yamashita, C. Coulon, and R. Clérac (2005). *J. Am. Chem. Soc.* **127**, 3090. (j) Y. Song, P. Zhang, X.-M Ren, X.-F. Shen, Y.-Z. Li, and X.-Z. You (2005). *J. Am. Chem. Soc.* **127**, 3708. (k) H. Miyasaka, H. Takahashi, T. Madanbashi, K. Sugiura, R. Clérac, and H. Nojiri (2005). *Inorg. Chem.* **44**, 5969. (l) C.-F. Wang, J.-L. Zuo, B. M. Bartlett, Y. Song, J. R. Long, and X.-Y. You (2006). *J. Am. Chem. Soc.* **128**, 7162. (m) T. Glaser, M. Heidemeier, T. Weyhermüller, R.-D. Hoffmann, H. Rupp, and P. Müller (2006). *Angew. Chem., Int. Ed.* **45**, 6033.
6. (a) J. L. Heinrich, P. A. Berseth, and J. R. Long (1998). *Chem. Commun.* 1231. (b) K. K. Klausmeyer, T. B. Rauchfuss, and S. R. Wilson (1998). *Angew. Chem., Int. Ed. Engl.* **37**, 1694. (c) K. K. Klausmeyer, S. R. Wilson, and T. B. Rauchfuss (1999). *J. Am. Chem. Soc.* **121**, 2705. (d) M. Ramesh and T. B. Rauchfuss (2004). *J. Organomet. Chem.* **689**, 1425. (e) E. J. Schelter, A. V. Prosvirin, W. M. Reiff, and K. R. Dunbar (2004). *Angew. Chem., Int. Ed.* **43**, 4912.
7. (a) J. Y. Yang, M. P. Shores, J. J. Sokol, and J. R. Long (2003). *Inorg. Chem.* **42**, 1403. (b) E. J. Schelter, A. V. Prosvirin, and K. R. Dunbar (2004). *J. Am. Chem. Soc.* **126**, 15004. (c) D. Li, S. Parkin, G. Wang, G. T. Yee, R. Clérac, W. Wernsdorfer, and S. M. Holmes (2006). *J. Am. Chem. Soc.* **128**, 4214. (d) D. Li, S. Parkin, R. Clérac, and S. M. Holmes (2006). *Inorg. Chem.* **45**, 7569.
8. (a) P.A. Berseth, J. J. Sokol, M. P. Shores, J. L. Heinrich, and J. R. Long (2000). *J. Am. Chem. Soc.* **122**, 9655. (b) M. P. Shores, P. A. Berseth, and J. R. Long (2004). *Inorg. Syn.* **34**, 149.
9. M. P. Shores, J. J. Sokol, and J. R. Long (2002). *J. Am. Chem. Soc* **124**, 2279.
10. (a) S. Wang, J.-L. Zuo, H.-C. Zhou, H. J. Choi, Y. Ke, J. R. Long, and X.-Z. You (2004). *Angew. Chem. Int. Ed.* **43**, 5943. (b) L. Jiang, H. J. Choi, X.-L. Feng, T.-B. Lu, and J. R. Long (2007). *Inorg. Chem.* **46**, 2181. (c) T. D. Harris and J. R. Long (2007). *Chem. Commun.*, 1360.
11. B. Mayoh and P. Day (1976). *J. Chem. Soc., Dalton Trans.* 1483.
12. G. M. Sheldrick, *Program for Empirical Absorption Correction of Area Detector Data* (University of Göttingen, Göttingen, Germany, 1996).
13. G. M. Sheldrick, *Program for Crystal Structure Refinement* (University of Göttingen, Göttingen, Germany, 1997).

14. (a) D. F. Shriver, S. A. Shiver, and S. E. Anderson (1965). *Inorg. Chem.* **4**, 725. (b) D. B. Brown, D. F. Shriver, and L. H. Schwartz (1968). *Inorg. Chem.* **7**, 77. (c) D. B. Brown and D. F. Shriver (1969). *Inorg. Chem.* **8**, 37. (d) J. E. House, Jr. and J. C. Bailar, Jr. (1969). *Inorg. Chem.* **8**, 672. (e) E. Reguera, J. F. Bertrán, and L. Nuñez (1994). *Polyhedron* **13**, 1619. (f) B. S. Lim and R. H. Holm (1998). *Inorg. Chem.* **37**, 4898 and references therein.
15. A. Bondi (1964). *J. Phys. Chem* **68**, 441.
16. (a) J. M. Williams, A. J. Schultz, A. E. Underhill, and K. Carneiro, *in* J. S. Miller (ed.), *Extended Linear Chain Compounds* (Plenum Press, New York, 1982), pp. 73–118 and references therein. (b) J. M. Willians (1983). *Adv. Inorg. Chem. Radiochem.* **26**, 235 and references therein.
17. (a) G. Marangoni, B. Pitteri, V. Bertolasi, V. Ferretti, and G. Gilli (1987). *J. Chem. Soc., Dalton Trans.* 2235. (b) A. J. Deeming and A. E. Vassos (1997). *J. Chem. Soc. Dalton Trans.*, 3519. (c) C.-H. Chen, Y.-S. Chang, C.-Y. Yang, T.-N. Chen, C.-M. Lee, and W.-F. Liaw (2004). *J. Chem. Soc., Dalton Trans.* 137. (d) W. Stüer, B. Weberndörfer, J. Wolf, and H. Werner (2005). *J. Chem. Soc., Dalton Trans.* 1796.
18. L. M. C. Beltran and J. R. Long, work in progress.